# Aeromagnetic mapping of basement structures and gold mineralization characterization of Kirk range area, southern Malawi

Joshua Chisambi [a, *], Tiyamike Haundi [a], Bjorn Von der Heyden [b]

[a] Department of Mining Engineering, Malawi University of Business and Applied Sciences
[b] Department of Earth Sciences, Stellenbosch University, South Africa

## ABSTRACT

A high-resolution aeromagnetic survey was conducted in the Kirk Range region in southern Malawi to obtain comprehensive geological and structural information. This newly collected data was analyzed and interpreted to gain a better understanding of the mode of occurrence of gold mineralization and related structural characteristics. To understand the distribution of magnetic sources, many analytic approaches were applied to the aeromagnetic data, including reduction to the pole, Euler deconvolution, Spectrum analysis, and Tilt and Vertical Derivatives filtering. Spectral analysis and Euler deconvolution were used to determine the depth of magnetic sources. The study reveals that the studied region is characterized by NE-SW and roughly E-W direction structures and that the gold occurrence is restricted within these structures, implying that mineralization is structurally controlled. These structures are found at depths of 200-1000 meters, according to Euler solutions produced from this work. Based on the calculated depths the structures controlling mineralization, in the Kirk Range are interpreted to occur at a depth range of 200 to 1000m, and the trend of the structure in the NE-SW and E-W directions. However current gold mining is taking place at a fairly shallow depth of fewer than 50m and no gold mine has gone deeper than that. The structural pattern and depth extent estimations show that gold mineralization in the Kirk range is expected to continue up to 1000 meters because the majority of the structures controlling mineralization in the region are located within that depth range. It is therefore recommended that future exploration should go deeper to a depth of about 200-1000 meters or more focusing on these NE-SW and E-W structures because it is expected that at that depth range more mineralization should be intercepted.

Keywords: Kirk range area, Aeromagnetic anomaly, Geological structures, Mineral exploration.

## 1. Introduction

In the last century, solid mineral exploration using traditional geological mapping methods has produced excellent results. Some of the outcomes achieved by using the traditional geological methods in mineral exploration include working exploration models and an understanding of the geology and process of ore deposit formations. However, most geological settings are characterized by a high level of structural complexity, in which mineralization may be multi-stage or may be overprinted or remobilized during progressive stages in the evolving orogenic cycle [1]. This high degree of structural geological complexity complicates modern-day exploration efforts. The difficulty in discovering new ore resources requires a transition in exploratory activity from traditional geological methods to integrated exploration, which combines geophysics with traditional geological methods [2]. In regional geological analysis and mineral resources surveys, it is well known that geological structures are important because they provide ideal conditions for magma emplacement, and fluid migration, and can concentrate on economic mineralization in a variety of geodynamic settings. Therefore the identification and understanding of the structural fabric of the basement rocks are very critical in mineral exploration [2]–[11]. An important geophysical method for determining the regional geological structures of basement terrains is an airborne magnetic survey [4].

This is because several geological structures that are important in the formation of mineralized systems may not be visible from surface geology mapping and magnetic prospecting techniques may be used to map these hidden structures [12].

In recent years, high-resolution aeromagnetic surveys have been widely used in mineral exploration and have proven to be an especially useful geophysical method in studying geological structures. For example authors in [5] analyzed the geological structures and the distribution pattern of polymetallic deposits of the eastern Tianshan, using aeromagnetic and gravity data. They found that structures trend E-W, NEE, and NW. Furthermore, the authors in [3] used aeromagnetic data to better understand the geology and mineral resources near the late Carboniferous-late Permian porphyry Cu-Mo polymetallic mineralization in the Chinese Eastern Tianshan. Using this technique, they found five prominent Cu-Mo positive anomalies.

In this study, we acquired high-resolution magnetic data for the Kirk range area in southern Malawi. The Kirk Range is one of the well-known gold occurrences in Malawi. Gold has been known to occur in the Kirk Range Lisungwe valley since 1908 and was first reported by Andrew and Bailey [13]. Artisanal miners mine gold in this area, which is primarily alluvial. Even though the Kirk Range contains several alluvial gold workings, there is little information on the structures that control primary mineralization and the depth extent of these structures remains sparse. Authors in [14] and [15]conducted a first insight detailed study regarding gold mineralization in the area. They report that mineralization in the Kirk Range occurs in linear structures in the form of veins and stringers. Since mineralization occurs primarily in veins and linear structures, the aeromagnetic method can be used to delineate

---

them in terms of depth, pattern, and aerial extent. In this study, aeromagnetic data were analyzed to delineate the structural lineaments distribution within the Kirk Range according to their spatial and directional attributes as well as define the depth of magnetic causative bodies and how these structures may be used to identify regions that are conducive to further exploration. This research will help us gain a better understanding of the area and will serve as a reference for future gold prospecting into other similar gold occurrence sites in Malawi. The use and study of aeromagnetic data to delineate structures has long served as a basis for regional structural controls of mineralization in many ore deposits and allows for more accurate targeting of structures interrelated with mineralization, [16].

### 1.1. Geologic setting

The Kirk Range is a medium to high-metamorphic grade mobile belt which is related to the Southern Irumide orogeny. It is located between 15.30° S and 15.31° S latitudes and 34.82° E and 34.85° E longitudes. The geology of the Kirk Range, and indeed the entire country of Malawi, is poorly understood, with the oldest geological map dated 1965 [13].

Malawi's geology is underlain by Malawi basement complex rocks, which are high-grade metamorphic para- and orthogneisses and schists and are of the Precambrian to lower Paleozoic periods [17]. These rocks have experienced high-grade metamorphism and polyphase deformation, as well as a protracted structural and metamorphic history [18]–[20]. Three important orogenic events have affected these rocks (Ubendian, Irumide, and Mozambiquean),[21].

The Ubendian orogenic event was first described by authors in [22] and is characterized by NW-SE trending structures. It occurred between 2200 and 1800 Ma during the Palaeoproterozoic Ubendian Orogeny [23]. The rocks of the Ubendian belt are characterized by sequences of medium to high-grade metamorphic supracrustal gneisses and schist that were intruded by various plutonic igneous rocks [24]. Peak metamorphic conditions of 750-850°C at 18 kbar were recorded in the rocks, as well as high-pressure granulite facies conditions [21]. During the Mesoproterozoic (Irumide) and Neoproterozoic (East African/Pan-African) orogenies, the Ubendian belt rocks were structurally overprinted. These subsequent events significantly affected the belt's interior architecture, obscuring the Ubendian Palaeoproterozoic history.

Mesoproterozoic Irumide orogeny is a northeast-trending orogenic belt. It is distinguished by a rapid change in metamorphic grade from greenschist to granulite facies. Authors in [24] and [25] were the first to describe the Irumide Belt and its dominant structural trend is northeast. This orogenic belt is subdivided into the Irumide Senso Stricto, the Southern Irumide, the Unango Subprovince, and the Nampula Subprovince with a general trend of NE-SW [27].

The regional metamorphic grade in the Irumide Belt is of medium pressure/medium temperature Barrovian type, which is more consistent with an accretionary setting than a continent-continent collision. The timing of peak metamorphism in the Irumide belt constrained by SHRIMP U–Pb zircon dates between $1021 \pm 16$ and $1018 \pm 5$ Ma [28]. P–T–t models. suggest a clockwise metamorphic P–T–t path [29] that is linked to the major shortening event recorded by northwest-verging thrusts.

Malawi's final major orogenic event, the Pan African Orogeny, occurred about 800-500 Ma, resulting in extensive overprinting of prior orogenic features from the Ubendian- and Irumide orogenies[24]. The orogenic event's peak temperatures were estimated to be 750-800°C at 12-13 kbar, and amphibolite facies retrogression occurred at 550-700°C at 5-8 kbar [29]. This Pan African Orogeny reactivated older pre-existing structures and formed new N-S trending structures. The regional geological map is shown in Figure 1.
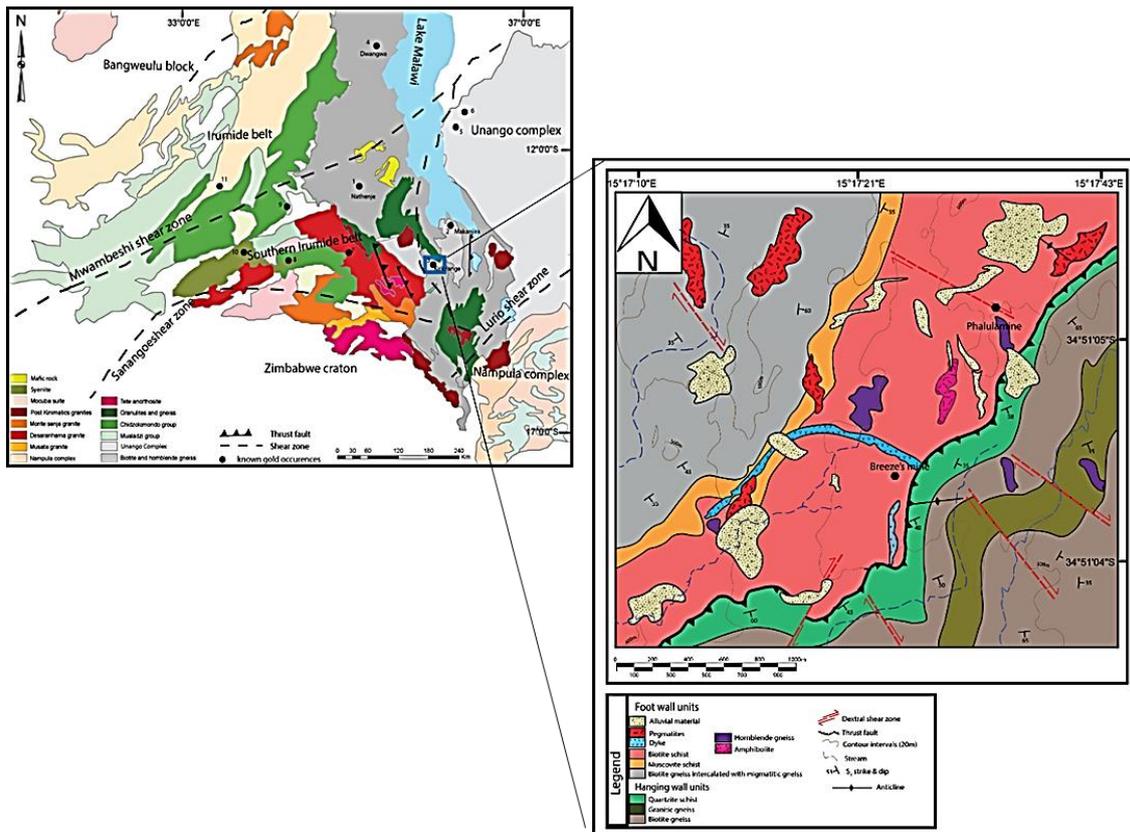


**Figure 1:** Regional geology for southern Malawi and surrounding countries. Our study area is located in the blue rectangle. Figure 1b, a detailed geology map of the study area (Blue rectan-gle) adapted from authors in [30].

## 2. Materials and Methods

Sander Geophysics Limited (SGL) used a Cessna Grand Caravan 208B aircraft to undertake a fixed-wing high-resolution airborne magnetic survey in Malawi for the Government of the Republic of Malawi's Ministry of Mining. The aircraft was equipped with a high-resolution airborne magnetometer. The survey was conducted with survey traverse lines oriented northeast-southwest at N45°E and spaced at 250m, with orthogonal control lines spaced at 5,000m. The aeromagnetic intensity data were processed using Geosoft Oasis MontajTM software. The airborne magnetometer data were corrected for IGRF using the position, altitude, and date of each point. The IGRF values were determined using the IGRF model from 2010. The DGPS heights above the GRS-80 ellipsoid were used for the IGRF corrections.

The original data lines were gridded using a minimum curvature gridding method and a 50 m grid cell size was employed. Because of the difference in the earth's magnetic field at the measurement spot, magnetic anomalies frequently have complex shapes. To solve this, the total magnetic field was reduced to the pole (RTP) using the reduction to the pole algorithm[31]. RTP positions the anomalies more directly over their causative bodies, and hence makes interpretation easier [32].

Euler deconvolution technique was used to provide a depth estimate of Magnetic Sources over the study area. This approach delineates the geometry of magnetic bodies using structural indices (SI) and is based on Euler homogeneous equation [33].

$$(x - x_0)\frac{\partial T}{\partial x} + (y - y_0)\frac{\partial T}{\partial y} + (z - z_0)\frac{\partial T}{\partial z} = N(B - T) \qquad (1)$$

where $(x_0, y_0, z_0)$ is the location of a magnetic source whose total field is observed at $(x, y, z)$, $\frac{\partial T}{\partial x} \frac{\partial T}{\partial y}$ and $\frac{\partial T}{\partial z}$ are derivatives of the magnetic field in the x, y, and z respectively while B is the value of the regional value of the total field. The homogeneity degree N is construed as a structural index [34].

The structural index SI defines the anomaly attenuation rate at the observation point and depends on the nature of the field source. The RTP aeromagnetic data were used for calculation of the Euler's deconvolution solutions using structural indices (SI) of 0, 0.5, 1, 2, and 3 and a window size of 10 × 10. "A window size of 10 × 10" means a squared window with a dimension of 10 * 50 m = 500m (10 × cell size).

An upward continuation filter of 100m was applied to the aeromagnetic data before computing the Euler deconvolution in order to get rid of the short-wavelength cultural noise.

Tilt, and Vertical derivatives as well as Analytic signals are among the other methods of data enhancement that were applied to the RTP magnetic data. Tilt and Vertical derivatives assisted in evaluating lineaments and the analytic signal was used to delineate the edges of the magnetic anomalies [10].

## 3. Results and Discussion

### 3.1. Reduced to Pole Total Magnetic Intensity map: Geological implications

The RTP was carried out because it places the anomalies more immediately over their causative bodies, making interpretation easier [32]. Due to variations in the earth's magnetic field at the spot of measurement, magnetic anomalies frequently have complex shapes. The RTP was performed using an inclination, I, of $-50^0$ and a declination, D, of $-6.4^0$ employing the International Geomagnetic Reference Field (IGRF), epoch 31st May 2020. Fig 2a displays the RTP's output, which exhibits high-amplitude, long-wavelength anomalies trending in the NE-SW and E-W directions in the northeastern and central regions of the study area. Deeper magnetic sources are suggested by these high magnetic anomalies. On the surface, biotite gneiss, biotite schist, granitic gneiss, and quartzite schist units on the northeastern side coincide with NE-striking magnetic highs. Similar amplitude anomalies can be detected on the eastern and southwestern sides, corresponding to granitic gneiss and biotite schist exposures.

Longer wavelength anomalies linked with these units point to deeper underlying magnetic sources attributed to intrusive bodies, which could have served as a heat source for gold mineralization. On the northwestern, southeastern, and central parts, charnockitic gneiss, feldspathic gneiss, and muscovite schist units coincide with the magnetic lows. The low magnetic fingerprints could indicate that large changes in rock magnetism have occurred in these units as a result of hydrothermal alteration.

### 3.2. The Analytic Signal Map

The analytic signal map was calculated in Oasis Montaj software from the total magnetic intensity (Fig. 2b). This enhancement was made because it provides a much-improved resolution of prominent magnetic boundaries [35] and it was used to delineate the edges of the magnetic anomalies. Analysis of the analytic signal map (Fig. 2b) revealed the existence of various anomaly peaks and boundaries of the biotite gneiss rocks and granite. Anomalies with high magnitude in the eastern part of the study area are related to granitic gneiss and biotite gneiss.

Prominent linear structures on the center trending NE-SW and E-W can be seen from the analytic signal map. These elongated linear features which show a high magnetic signature are associated with faults that acted as conduits for mineralizing fluids.

### 3.3. Tilt and Vertical Derivatives Maps

The geological structures in the region are depicted on the Tilt and Vertical derivative maps. The data on derivatives enables the identification of dominant linear trends in the Lisungwe Valley (Fig. 2). Faults and deep-level basement shear zones are thought to be represented by these linear structures. According to the aeromagnetic data, the Kirk range has substantial faulting and shearing and the NE-SW structural grain is the most prominent structural grain in the region. These major fractures may have served as a plumbing system for mineralizing hydrothermal fluids and played an important role in gold mineralization.

The NE-SW trending faults and shear zones are more clearly depicted on the Tilt Derivative map. The central part of the Kirk range area is marked by an increase in visibility of shallow structural features. The first vertical derivative map and Tilt derivative map (Figs. 2c, d) indicate a significant improvement in the visibility of structural features, especially in the central and NE sections, when compared to the total field map (Fig. 2a). These structures are thought to have served as conduits for hydrothermal fluids. The geology of the Kirk range is therefore associated with` these NE-SW trending regional structures/faults, according to geophysical evidence presented in this study.

### 3.4. Gold Mineralization

Breeze Au mine and Phalula Au mine are two historical gold mines in this study area (orange dots in Figure 2). These historic gold mines are located along these NE-SW structures identified in the airborne geophysical data. The majority of gold occurrences in the Kirk range occur along with these structures as well (Figure 2 c,d). The proximity of historical gold mines and gold occurrences to the structures implies a strong relationship, suggesting that these structures (shear zones and faults) may have served as potential fluid channels for hydrothermal fluids.

### 3.5. Estimation of Depth

#### 3.5.1. Spectral analysis

The spectral investigation was carried out by applying a power spectrum method to calculate the depth of magnetic sources, which provides a degree of the overburden thickness. The use of the power spectrum to estimate the depths of magnetized bodies is a well-established process [36], [37]. To estimate the source depth, the data is transformed in the frequency domain through the Fourier transform
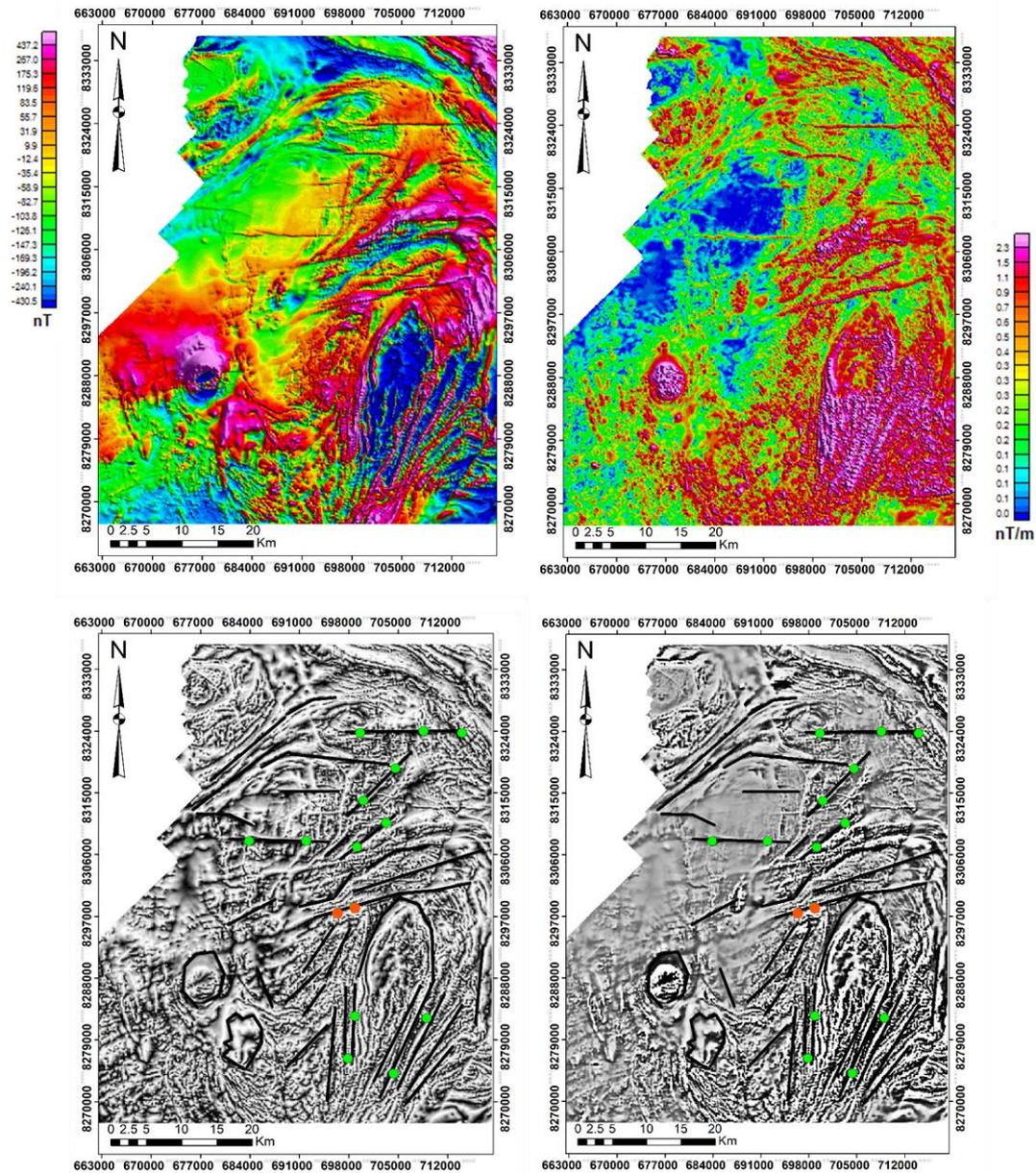
**Figure 2**: Airborne geophysical data of the Kirk range area with interpreted linear structures overlain on it, (a) Total Magnetic Intensity Image (b) Analytic signal (c) Tilt derivative image, and (d) Vertical derivative, orange dots operating gold mines, green dots, gold occurrences. Gold mines and known gold occurrences are spatially correlated with the linear structures.

and then the power spectrum is taken from the square of the Fourier amplitude spectrum. A plot between the log of the power spectrum and the wavenumber fits a straight line. One-half of the slope value of the fitted straight line gives the depth of the anomalous body [38]. This statistical method has been found to produce accurate magnetic basement depth estimates [39].

The spectral analysis of the Kirk Range suggests deeper sources lie at depth of 3.14 km. Conversely, the shallower magnetic bodies lie between 100 m and 1.1 km (Figure. 3). The deep magnetic sources are thought to come from the region's magnetic basement. The depths determined by the spectral analysis were correlated with the depths determined by Euler deconvolution.

### 3.5.2. The Euler deconvolution

Using Euler deconvolution analysis, we approximated the depths of magnetic susceptibility sources. Unlike the power spectrum method, the Euler deconvolution method has parameters that must be set in order

to achieve significant depth results [34]. The window size determines the maximum source depths by applying the Euler equation to a specific location. Maximum depths are generally twice the window size [34], and we observed that utilizing window sizes between 10 x 10 yielded optimal solutions. Structural index = 1 (i.e., SI=1) best matched the source geometries within the region based on the local geology.

The solution results of SI=1 were plotted on the Tilt derivative shaded relief map (Figure 4b) for effective correlation and the solutions correlate with the structures identified in Figure 2. Figure 4 shows that the solutions plot cluster along with the geological structures (lineaments) on the Tilt derivative map. The depth solution locations provide distribution characteristics of edges of magnetized bodies and fault structures, as well as more deep information about geological structures that are not reflected in surface geology.

According to the structural pattern and depth scale estimates inferred from magnetic anomalies, Euler solutions suggest deeper sources lie at 3.2 km depth and the shallower magnetic bodies lie between 100 m and

1000 m (Figure 4). These depth estimates correlate very well with those obtained using spectral analysis.

Most structures occur at a depth range of 200 to 1000m and they trend in the NE-SW and E-W directions. The interpretation results show that the NE-SW and E-W-trending structures are extensively developed in the study area. These structures may be regarded as lineaments/faults that host viable gold mineralization in the area. These structures are interpreted to represent major fractures within the study area that served as a conduit for mineralizing fluid. We have plotted the known locations of old gold mines and gold occurrences in figure 2. The location of these old gold mines and gold occurrences mostly occurs along with these NE-SW structures and coincides with the Euler solutions suggesting that mineralization is structurally controlled and goes deeper. This signifies that significant mineralization lies at this depth range within the region, mainly within these NE-SW and E-W trending structures.

Quartz vein systems mineralized with economic grades of gold were previously mined at Breeze and Phalula mines.

Geological Survey of Malawi drilled a 200 m hole close to Breeze mine and we cut part of the drill core samples and made thick sections which were observed under reflected light microscopy (Figure 5 d). From the drill core samples derived from boreholes, ubiquitous gold grains are identified by reflected light microscopy. Mineralization is associated with sulfide mineral assemblages dominated mainly by pyrite, pyrrhotite, and chalcopyrite (Figure 5 abc). Gold is present both as free Au in wall rock and associated with pyrite. Predominantly gold is hosted in biotite schists and gneisses and is associated with a sulfide mineral paragenesis. Significant mineralization was intercepted from the depth of 150m and continues to over 200m. Our hole did not go beyond 200m but mineralization continues over 200m depth.

However, field studies of the artisanal mines at Breeze and Phalula mines show that most of the gold mining occurs at a depth range of 2 to 50 m. The deepest mine goes up to 50m. Based on the depths suggested by structures controlling mineralization, mining is at present occurring at very shallow depths. By implication, some mineralized veins are still lying below the present mining depth of less than 50 m.

The possibility of finding more gold by exploring at a greater depth is high because the depth extent estimates and structural pattern reveal that substantial structures controlling mineralization within the Kirk range occur at much higher depths mainly along NE-SW and E-W trending structures. It is therefore recommended that future exploration should go deeper to a depth of about 200-1000 meters or more. Regional structures as well as mineralized quartz-sulfide vein sets exhibit a NE-SW and E-W trend which is consistent with the fabric observed with the airborne magnetics [40]–[42].
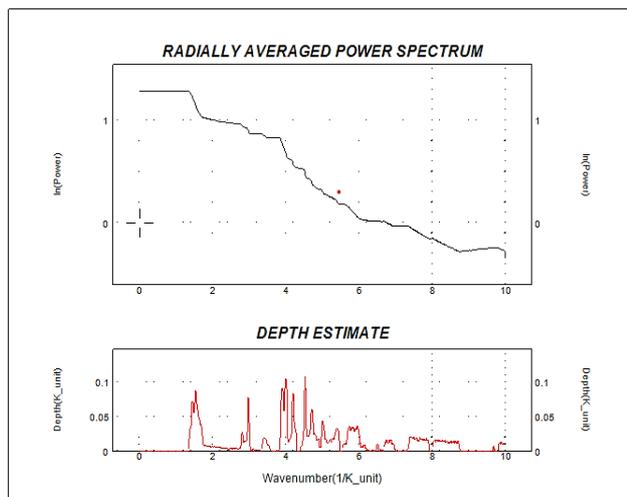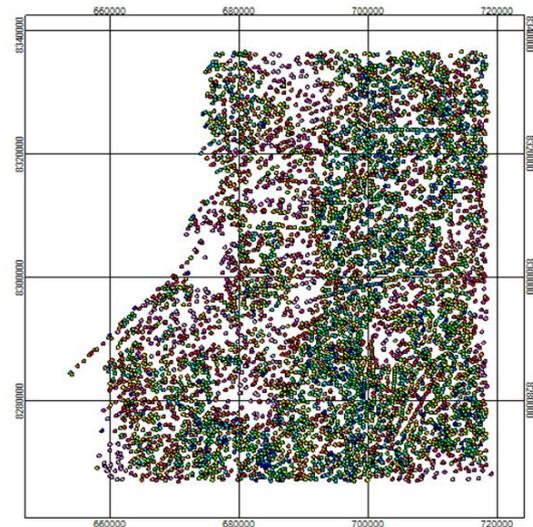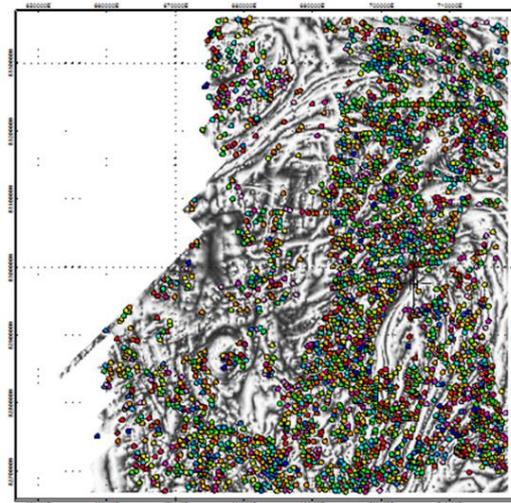


**Figure 3.** Radially averaged Power spectrum for the Kirk range magnetic data indicating depth estimates of magnetized bodies.



(a)



(b)



**Figure 4:** Euler solutions with a structural index of 1. Most linear structures in figure 2 are depicted by the solutions. The Euler depth range from 200 to 1000m.

Structural indices of 2 and 3, which indicate a pipe, sphere, or ring-like massive anomalous body, lacked a definite solution., this could indicate that the ore bodies are dispersed.

## 4. Conclusions

Newly acquired airborne magnetic data of the Kirk range area has been analyzed and interpreted. This study has found that the Kirk range is dominated by NE-SW and E-W structures that control gold mineralization in the area. Obtained Euler solutions from this work reveal that most of these structures occur at a depth range of 200 to 1000m. The known gold occurrences and gold mines in the Kirk range have a significant correlation with these structures. These are the structures that control primary gold mineralization in the Kirk Range and are prospective for future gold exploration. Current gold mining is occurring at shallow depths and the structures controlling mineralization continue up to a depth of 200-1000m which means that most gold mineralization is laying underneath therefore future further exploration should target these deep structures which could be proved by drilling.
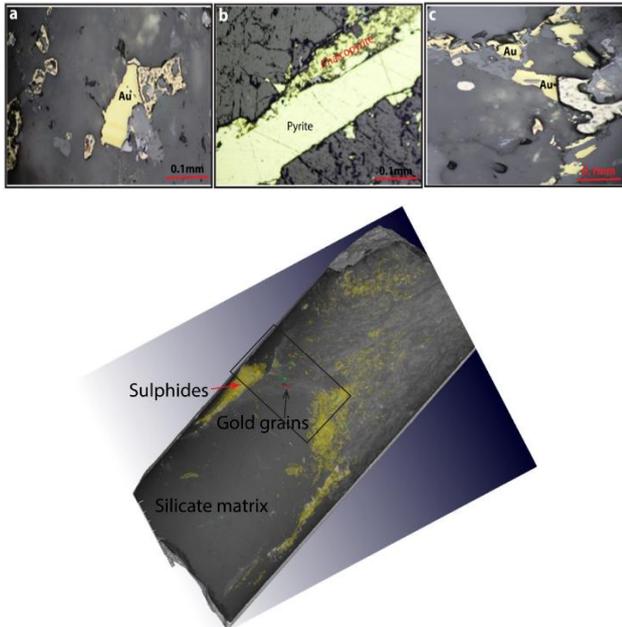
**Figure 5:** Thin sections observed in reflected light microscopy indicating the presence of gold mineralization at a depth of 170m.(a) Thin section indicating gold and pyrrhotite (b) Thin section indicating Pyrite and Chalcopyrite (c) Thin section indicating gold and pyrite (d) drilled core sample at 170m depth with gold mineralization. The core sample was cut on the rectangles shown and made into thin sections. This core sample was scanned using XCT the yellow are sulfides, the dark-colored is silicate matrix and the warm colors are gold grains (red big grains, green medium grains, and blue small grains) identified based on density.

## Acknowledgments

## REFERENCES

[1] Augustin,J and D. Gabour, "Multi-stage and multi-sourced fluid and gold in the formation of orogenic gold deposits in the world-class Mana district of Burkina Faso − Revealed by LA-ICP-MS analysis of pyrites and arsenopyrites," *Ore Geol. Rev.,* 2019.

[2] W. S. Ibrahim, K. Watanabe, and K. Yonezu, "Structural and litho-tectonic controls on Neoproterozoic base metal sulfide and gold mineralization in North Hamisana shear zone, South Eastern Desert, Egypt: The integrated field, structural, Landsat 7 ETM+ and ASTER data approach," *Ore Geol. Rev.,* vol. 79, pp. 62–77, 2016, doi: 10.1016/j.oregeorev.2016.05.012.

[3] F. Xiao and Z. Wang, "Geological interpretation of Bouguer gravity and aeromagnetic data from the Gobi-desert covered area , Eastern Tianshan , China : Implications for porphyry Cu-Mo polymetallic deposits exploration," *Ore Geol. Rev.,* vol. 80, pp. 1042–1055, 2017, doi: 10.1016/j.oregeorev.2016.08.034.

[4] Hassanein H and Soliman, "Aeromagnetic data interpretation of Wadi Hawashiya area for identifying surface and subsurface structures, northeastern desert, Egypt.," *J. KAU Earth Sci 20(1)117–139,* 2009.

[5] S. An *et al.*, "Interpretation of high resolution aeromagnetic data for structures study and exploration of polymetallic deposits in Kalatage area, eastern Tianshan (NW China)," *Geosci. J.,* vol. 24, no. 3, pp. 315–327, 2020, doi: 10.1007/s12303-019-0027-6.

[6] A. A. Akinlalu *et al.*, "Aeromagnetic mapping of basement structures and mineralisation characterisation of Ilesa Schist

Belt, Southwestern Nigeria," *J. African Earth Sci.,* vol. 138, pp. 383–391, 2018, doi: 10.1016/j.jafrearsci.2017.11.033.

[7] A. Shaole, K. Zhou, J. Wang, H. Yang, and Z. Zhang, "Integrated analysis of gravity and magnetic fields in the Eastern Tianshan Belt, Xinjiang, Central Asia: Implications for Cu-Au-Fe polymetallic deposits exploration," *J. Appl. Geophys.,* vol. 159, pp. 319–328, 2018, doi: 10.1016/j.jappgeo.2018.09.002.

[8] N. Olasunkanmi, O. Bamigboye, O. Saminu, N. Salawu, and T. Bamidele, "Interpretation of high resolution aeromagnetic data of Kaoje and its environ, western part of the Zuru Schist belt, Nigeria: implication for Fe–Mn occurrence," *Heliyon,* vol. 6, no. 1, p. e03320, 2020, doi:.1016/j.heliyon. 2020.e03320.

[9] M. A. Oladunjoye, A. I. Olayinka, M. Alaba, and M. A. Adabanija, "Interpretation of high resolution aeromagnetic data for lineaments study and occurrence of Banded Iron Formation in Ogbomoso area, Southwestern Nigeria," *J. African Earth Sci.,* vol. 114, pp. 43–53, 2016, doi: 10.1016/j.jafrearsci.2015.10.015.

[10] J. Wang and X. Meng, "An aeromagnetic investigation of the Dapai deposit in Fujian Province, South China: Structural and mining implications," *Ore Geol. Rev.,* vol. 112, no. August, p. 103061, 2019, doi: 10.1016/j.oregeorev.2019.103061.

[11] A. Miftah *et al.*, *Combined analysis of helicopter-borne magnetic and stream sediment geochemical data around an ancient Tiouit gold mine (Eastern Anti-Atlas, Morocco): Geological and mining interpretations,* vol. 175. Elsevier Ltd, 2021.

[12] C. J. Chernicoff, J. P. Richards, and E. O. Zappettini, "Crustal lineament control on magmatism and mineralization in northwestern Argentina: geological, geophysical, and remote sensing evidence," *Ore Geol. Rev.,* vol. 21, pp. 127–155, 2002.

[13] Bloomfield.K and Garson.M.S, "The Geology of the Kirk Range-Lisungwe Valley Area. Ministry of Natural Resources. Geological Survey Department. Bulletin No.17.," *Gov. Printer, Zomba. Malawi,* 1965.

[14] J. Chisambi and B. von der Heyden, "Primary gold mineralization in the lisungwe valley area, kirk range, southern Malawi," *South African J. Geol.,* vol. 122, no. 4, pp. 505–518, 2019, doi: 10.25131/sajg.122.0039.

[15] J. Chisambi, T. Haundi, and G. Tsokonombwe, "Geologic structures associated with gold mineralization in the Kirk Range area in Southern Malawi," *Open Geosci.,* vol. 13, no. 1, pp. 1345–1357, 2021, doi: 10.1515/geo-2020-0304.

[16] M.-L. Airo and S. Mertanen, "Magnetic signatures related to orogenic gold mineralization, Central Lapland Greenstone Belt, Finland," *J. Appl. Geophys.,* vol. 64, no. 1–2, pp. 14–24, Mar. 2008, doi: 10.1016/j.jappgeo.2007.10.003.

[17] G. S. Carter, "THE GEOLOGY AND MINERAL RESOURCES OF MALA WI." Government print, Zomba, Malawi, 1973.

[18] and D. Z. Chipili., E., "'The Geology of the North Kirk Range. Ministry of Energy and Mining. Geological Survey Department. T1228A.,'" 1997.

[19] E. Chipili. and Dulanya.Z, "The Geology of the North Kirk Range. Ministry of Energy and Mining. Geological Survey Department. T1228A.," 1997.

[20] Z. Dulanya, N. Morales-simfors, and Å. Sivertun, "Journal of African Earth Sciences Comparative study of the silica and cation geothermometry of the Malawi hot springs : Potential alternative energy source," *J. African Earth Sci.,* vol. 57, no. 4, pp. 321–327, 2010, doi: 10.1016/j.jafrearsci.2009.11.001.

[21] U. Ring, A. Kröner, and T. Toulkeridis, "Palaeoproterozoic

granulite-facies meta-morphism and granitoid intrusions in the Ubendian-Usagaran Orogen ofnorthern Malawi, east-central Africa.," *Precambrian Reserch.*, vol. 85, 27–51., 1997.

[22] R. B. McConnell, *Outline of the geology of Ufipa and Ubende. Bulletin of Geological Survey of Tanganyika.* 1950.

[23] S. Dewaele, P. Muchez, R. Burgess, and A. Boyce, "Geological setting and timing of the cassiterite vein type mineralization of the Kalima area ( Maniema , Democratic Republic of Congo )," *J. African Earth Sci.*, vol. 112, pp. 199–212, 2015, doi: 10.1016/j.jafrearsci.2015.09.006.

[24] J. L. et al Lenoir, "The Palaeoproterozoic Ubendian shear belt in Tanzania: geochronology and structure," *J. African Earth Sci.*, vol. 19, no. 3, pp. 169–184, 1995.

[25] E. H. Ackermann, "Ein neuer Faltengürtel in Nordrhodesien und seine tektonische Stellung im Afrikanischen Grundgebirge.," *Geol. Rundschau*, vol. 38, 24–39, 1950.

[26] E. H. Ackermann and A. Forster, "Grundzuge der Stratigraphie und Struktur des Irumide Orogen.," *21st International Geological Congress,* pp. 182–192, 1960.

[27] P. H. Macey *et al.*, "Mesoproterozoic geology of the Nampula Block, northern Mozambique: Tracing fragments of Mesoproterozoic crust in the heart of Gondwana," vol. 182, pp. 124–148, 2010, doi: 10.1016/j.precamres.2010.07.005.

[28] B. De Waele, I. C. W. Fitzsimons, F. Tembo, and B. Mapani, "The geochronological framework of the Irumide Belt: A prolonged crustal history along the margin of the Bangweulu Craton *Am. J. Sci.*, no. February, 2009, doi: 10.2475/02.2009.03.

[29] B. De Waele and B. Mapani, "Geology and correlation of the central Irumide belt," *J. African Earth Sci.*, vol. 35, pp. 385–397, 2002.

[30] J. Chisambi and B. von der Heyden, "Primary gold mineralization at Manondo – Choma area, Kirk range, Southern Malawi," *South African J. Geol.*, no. 4, 2019.

[31] K. I. Kis, "Transfer properties of the reduction of magnetic anomalies to the pole and to the equator," *Soc. Explor. Geophys.*, vol. 55, no. 9, pp. 1141–1147, 1990.

[32] X. Li, "Magnetic reduction-to-the-pole at low latitudes: Observations and considerations," *Lead. Edge*, vol. 1, 2008.

[33] A. M. Aziz, W. A. Sauck, E.-A. H. Shendi, M. A. Rashed, and M. Abd El-Maksoud, "Application of Analytic Signal and Euler Deconvolution in Archaeo-Magnetic Prospection for Buried Ruins at the Ancient City of Pelusium, NW Sinai, Egypt: A Case Study," *Surv. Geophys.*, vol. 34, no. 4, pp. 395–411, Apr. 2013, doi: 10.1007/s10712-013-9229-z.

[34] Reid, A.B., Allsop, J.M., Granser, H., Millett, A.J. & Somerton, I.W., "Magnetic interpretation i n three dimensions using Euler deconvolution," *Geophysics,* vol. v 55, 80-9.

[35] M. Dobrin and C. H. Savit, "Introduction to Geophysical Prospecting," 1988. http://www.amazon.com/Introduction-Geophysical-Prospecting-Milton-Dobrin/dp/0070171963 (accessed Aug. 19, 2014).

[36] A. and F. S. G. Spector, "Statistical Models For Interpreting Aeromagnetic Data," *Geophysics*, 1969.

[37] J. Garcia-Abdeslem, "Inversion of the power spectrum from gravity anomalies of prismatic bodies," *Geophysics*, vol. 60, no. 6, pp. 1698–1703, 1995, doi: 10.1190/1.1443902.

[38] Nabighian M.N., "The analytic signal of two-dimensional mag-netic bodies with polygonal cross-section: its properties and use for automated anomaly interpretation.," *Geophys. 37, 507±517.*

[39] F. S. Spector, A. and Grant, "Statistical models for interpreting aeromagneflc data.," *Geophys. 35, 293- 302.*

[40] B. De Waele, A. Kampunzu, and F. Tembo, "The Mesoproterozoic Irumide belt of Zambia," *J. African Earth Sci.*, vol. 46, pp. 36–70, 2006, doi: 10.1016/j.jafrearsci.2006.01.018.

[41] R. Boyd *et al.*, "The Geology and Geochemistry of The East African Orogen In Northeastern Mozambique," *Geol. Soc. South Africa*, vol. 113, pp. 87–129, 2010, doi: 10.2113/gssajg.113.1.87.

[42] B. Bingen *et al.*, "Geochronology of the Precambrian crust in the Mozambique belt in NE Mozambique, and implications for Gondwana assembly," *Precambrian Res.*, vol. 170, pp. 231–255, 2009, doi: 10.1016/j.precamres.2009.01.005.